Available online at www.sciencedirect.com
SCIENCE DIRECT®
Chaos, Solitons and Fractals 31 (2007) 327–335
CHAOS SOLITONS & FRACTALS
www.elsevier.com/locate/chaos

Non-linear response of an electrode–electrolyte interface impedance with the frequency

G. Ruiz *, C.J. Felice

Departamento de Bioingeniería, UNT/CONICET, Argentina

Accepted 26 September 2005

Abstract

In this paper we analyze the frequency response of a distributed parameters non-linear circuit. This circuit is a fractal model of an electrode–electrolyte interface. The results show that the series equivalent resistance R_{eq} decreases as the number of fractal levels rises. Its frequency behavior is similar to the results described by other authors that used a constant phase angle element. At low frequency range, the series equivalent reactance X_{eq} decreases with frequency and R_{eq} shows a flat response in this range. The model also explains how interface geometry modifies the values of some electrochemical parameters. As roughness increases the Argand diagram shows smaller semicircles. The model behavior is like a single dispersion system with its central frequency increasing with the electrode roughness.

1. Introduction

Frequency dependence of an electrode impedance is not a new phenomenon. The electrode–electrolyte interface (EEI) was studied at low [1–10] and at high current density [7,11–13]. In non-linear dielectric spectroscopy of biological suspensions, the way EEI distorts the biological non-linearities was poorly studied [14–16].

A new EEI model which integrate in the same electrical circuit, electrochemical and geometrical features of an electrode, was presented previously in one of our papers. [13]. This model allows to predict qualitatively the EEI behavior at high and low current density and at constant frequency. The frequency response of the model above is presented in this paper.

Our results show that the series equivalent resistance R_{eq} of the circuit decreases when the number of fractal levels considered increases, and its frequency behavior is qualitatively similar to those reported by other authors [4,6,17] within the frequency ranges analyzed.

There is a significant similarity between our results and those presented by authors who used a constant phase angle (CPA) element [4,5,7,10,11] in their models.

The series equivalent reactance X_{eq} shows a *bell-like* behavior when the frequency decreases within the range analyzed, whereas R_{eq} shows a typical *sigmoid* curve. The model behave as if it were a single dispersion system. This also explains how the interface roughness might affect the quantification of pure electrochemical parameters.

* Corresponding author. Tel./fax: +54 381 436 4120.
E-mail address: gruiz@herrera.unt.edu.ar (G. Ruiz).

0960-0779/$ - see front matter © 2005 Published by Elsevier Ltd.
doi:10.1016/j.chaos.2005.09.064

2. Interfaces modelling

2.1. EEI fractal model

EEI was modeled as an electrical circuit originated in the geometrical structure of a fractal net, which includes two electrochemical parameters, the double layer capacity C_{dl} and the charge transfer resistance R_{ct} in parallel with C_{dl} as it is shown in Fig. 1 [13].

It is supposed that the charge transfer process is controlled by activation (neither the diffusion effects nor the mass transport by migration or convection are considered), in each electrochemical reaction one electron is transferred, and the corrosion or superficial adsorption processes are not considered either in order to simplify the procedure.

In Fig. 1 the value of the capacity and the charge transfer resistance of each level is obtained with the following equations:

$$C_{dlj} = 2^j C_{dl} \tag{1}$$

$$R_{ctj}(\eta_j) = \frac{1}{2^j J_0 \frac{F}{\Re T}\left((1-\beta_c)\exp\left[\frac{(1-\beta_c)F\eta_j}{\Re T}\right] + \beta_c \exp\left[\frac{-\beta_c F\eta_j}{\Re T}\right]\right)} \tag{2}$$

where J_0 is the exchange current density, F is the Faraday constant, $\Re$ is the universal gas constant, T is the absolute temperature, β_c is the cathodic transfer coefficient and j is the fractal level. If j is the 0 (fractal level 0) correspond to a flat electrode.

3. Series equivalent resistance and reactance for an EEI model of two fractal levels

The equivalent impedance for an EEI geometric model of two fractal levels is shown in Eq. (3),

$$Z_{eq} = R + \frac{Z_0\left(\frac{aR}{2} + \frac{Z_1(\frac{a^2R}{4}+Z_2)}{Z_1+\frac{a^2R}{4}+Z_2}\right)}{Z_0 + \frac{aR}{2} + \frac{Z_1(\frac{a^2R}{4}+Z_2)}{Z_1+\frac{a^2R}{4}+Z_2}} \tag{3}$$

where Z_j is a parallel between R_{ctj} and C_{dlj} and it is supposed that the apparent area of the working electrode is 1 cm^2, and $i = \sqrt{-1}$. The qualitative behavior with more levels is similar, and it does not contribute significantly to the understanding of the subject.

Finally,

$$R_{eq} = \mathrm{Re}(Z_{eq}) \tag{4}$$

$$X_{eq} = \mathrm{Im}(Z_{eq}) \tag{5}$$

4. Temporal evolution of R_{eq} and X_{eq} for an altern overpotential

When an altern overpotential η_{in} is applied on the interface (Eq. (6)), the overpotentials η_j, as well as R_{ctj} and C_{dlj}, with $j = 0, 1$ and 2, will also show periodical temporal behavior.

$$\eta_{in} = \eta_{in}^0 \sin(2\pi f t) \tag{6}$$

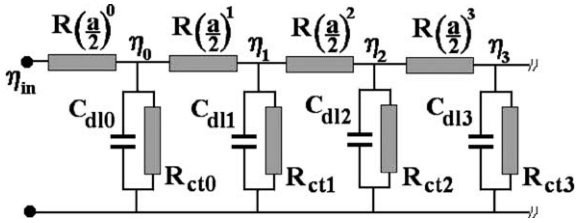

Fig. 1. Simplified fractal net of four branches showing the first fractals levels. R: electrolytical resistance, a: scale factor, $\eta_{0,1,2,3}$: overpotentials at different fractal levels.

In order to study the temporal evolution of R_{eq} and X_{eq}, the second Kirchoff's Law is applied (Eq. (7)) to the first node of the net in Fig. 1.

$$I_0 = I_1 + I_{R_{ct0}} + I_{C_{dl0}} \tag{7}$$

Given that

$$I_{C_{dl0}} = C_{dl0}\frac{d\eta_0}{dt} \tag{8}$$

It is obtained

$$\frac{d\eta_0}{dt} = \frac{\frac{\eta_{in}}{R} - \eta_0\left(\frac{1}{R} + \frac{1}{R_{ct0}} + \frac{2}{aR}\right) + \frac{2\eta_1}{aR}}{C_{dl0}} \tag{9}$$

By repeating the procedure on the next two nodes in the Fig. 1, the following expressions are obtained:

$$\frac{d\eta_1}{dt} = \frac{\frac{2\eta_0}{aR} - \eta_1\left(\frac{2}{aR} + \frac{1}{R_{ct1}} + \frac{4}{a^2R}\right) + \frac{4\eta_2}{a^2R}}{C_{dl1}} \tag{10}$$

$$\frac{d\eta_2}{dt} = \frac{\frac{4\eta_1}{a^2R} - \eta_2\left(\frac{4}{a^2R} + \frac{1}{R_{ct2}}\right)}{C_{dl2}} \tag{11}$$

Since R_{ctj} depend on the overpontentials η_j, Eqs. (9)–(11) are a differential equations system, which can not be solved analytically. Therefore, numerical method was applied and a simple algorithm was implemented in *Mathematica*.

5. Algorithm to obtain R_{eq} and X_{eq}

We started setting the values for J_0, $K = F/(\Re T)$, β_c, a, R, Δt, f, f_{max}, Δf, C_{dl} and η_{in}^0, and setting zero time t and overpotentials η_0, η_1 y η_2. Besides, at $t = 0$, $\eta_{in} = 0$ and $\eta_j = 0$ where $j = 0, 1$ and 2. With the previously defined values, R_{ctj} was calculated using Eq. (2), and $d\eta_j/dt$ using Eqs. (9)–(11). R_{eq} and X_{eq} were computed with the Eqs. (4) and (5) and they were saved into a data file including the initial values of η_j , R_{ctj}, $d\eta_j/dt$, R_{eq} and C_{eq}, at $t = 0$. A new iteration begins when time t and overpotential η_j are increased, and it is repeated until one period of the input signal is completed.

Once the cycles are completed, the Discrete Fourier Transform of R_{eq} and C_{eq} is calculated from the saved data, and another data file is created where the values of TDF(R_{eq}) and TDF(C_{eq}) are also saved, with the corresponding values of f and η_{in}^0. Then the program increase the frequency in Δf and it repeats the process above. Afterthat, the process is carried out again for other η_{in}^0 values.

For the simulation typical values of the parameters were used: $\beta_c = 0.5$, $T = 298$ K, $f = 1 \times 10^{-3}$ Hz, $f_{max} = 10^4$ Hz, $\eta_{in}^0 = 22$ mV, $R = 100\ \Omega$, $a = 4$, $C_{dl} = 1 \times 10^{-5}$ F, $J_0 = 2.1 \times 10^{-5}$ A/cm^2.

The Δf value chosen produced an uniform distribution of points in a logarithm scale.

With these values, the charge time of the capacitors is in the order of 10^{-3} s. For frequencies lower than 10^2 Hz the transient is negligible and a single input cycle is enough for the analysis. For frequencies higher than 10^4 Hz, the transient last 5 cycles, that is why 30 cycles were used for the averaging.

6. Materials and methods

In order to validate the proposed model, several experiments were carried out so as to study the ZIEE behavior with the frequency, at constant overpotential and using polished electrodes with sandpaper of different granulations.

The measurement cell (Fig. 2) is made of acrylic and it allows us to carry out tripolar measurements. The three electrodes are made of stainless steel DENTAURUM®. The working electrode (WE) is a solid cylinder (1.5 cm long), and only 1 cm^2 of its transversal section is exposed, the rest was insulated with grilon.

The counter electrode (CE) is semi circular and it was made with an area larger than the working electrode in order to minimize its impedance (70 cm^2). The reference electrode is 1 mm in diameter and only 1 mm is exposed at its end, the rest is covered with a glass sealed capillary. The measurements were carried out with the Solartron® system 12508 W which includes a Frequency Response Analyzer 1250 and an electrochemical interface 1287. The data

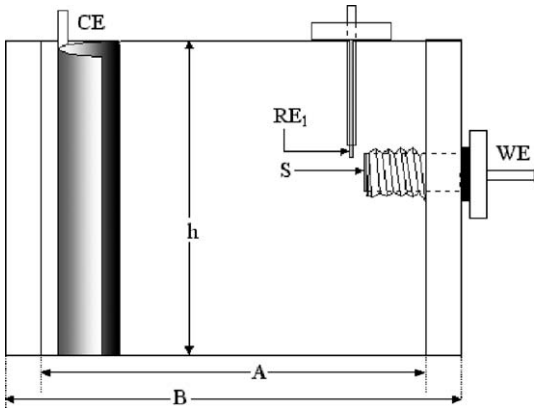

Fig. 2. Lateral view of the measurement cell. $A = 10.0$ mm, $B = 11.8$ mm, $h = 8.4$ mm, $S = 1$ cm^2.

Table 1
Steps for polishing electrodes

	Step 1	Step 2	Step 3	Final roughness (μm)
Electrode 1	sandpaper # 180 AcquaFlex®	sandpaper # 240 Carbimet®	sandpaper # 600 Carbimet®	25.80
Electrode 2	sandpaper # 180 AcquaFlex®	sandpaper # 240 Carbimet®		58.50
Electrode 3	sandpaper # 180 AcquaFlex®			78.00

The size of the grain matches the European standards FEPA standard 43-GB-1984 (R1993).

visualization and processing were carried out with the commercial systems Zplot® and Zview® of Solartron. The electrodes were polished in gradual steps and with different roughness degrees according to the diagram indicated in Table 1.

Overpotentials with frequencies within the interval of 0.01 to 65,000 Hz were applied with the Solartron system.

The sampling frequency was such that the measurements points were equally spaced in a logarithmic scale taking 10 points per decade. The integration time of the measurements was of 1 cycle for frequencies lower than 1 Hz and 16 cycles for the rest.

In every case, the potential was stabilized in open circuit until the voltage shift was lower than 0.05 mV/seg; then the equivalent series resistance and reactance measurements were carried out. The overpotentials used were 5, 20 and 50 mV. The working solution used was NaCl 0.9%.

7. Results

7.1. Theoretical

7.1.1. R_{eq} and X_{eq} as a function of the ac overpotential frequency

Fig. 3 shows the average temporal value of R_{eq} (a) and X_{eq} (b) as a function of the frequency of the overpotential applied, for three nets and each one corresponding to a different fractal level ($j = 0, 1, 2$). These values are evaluated through the DC components of the Fourier spectrum DFT(dc) of the R_{eq} and X_{eq}, curves for each frequency. Fig. 3 also shows a single frequency dispersion f_0, where X_{eq} presents a maximum, and this frequency f_0 increases with the increment of the interface roughness.

Another way to show the results of Fig. 3 is to represent $-iX_{eq}$ as a function of R_{eq} for each one of the frequencies (Argand diagram). This is shown in Fig. 4. The circular fitting of the rough electrodes, produces depressed semi-circular arc whose center lies below the real axis.

These fitting are not shown in order to clarify the figure. The flat electrode does not show any depression in the center of the circle, this event is well described in the literature of disperse systems [4,5]. When the roughness increases,

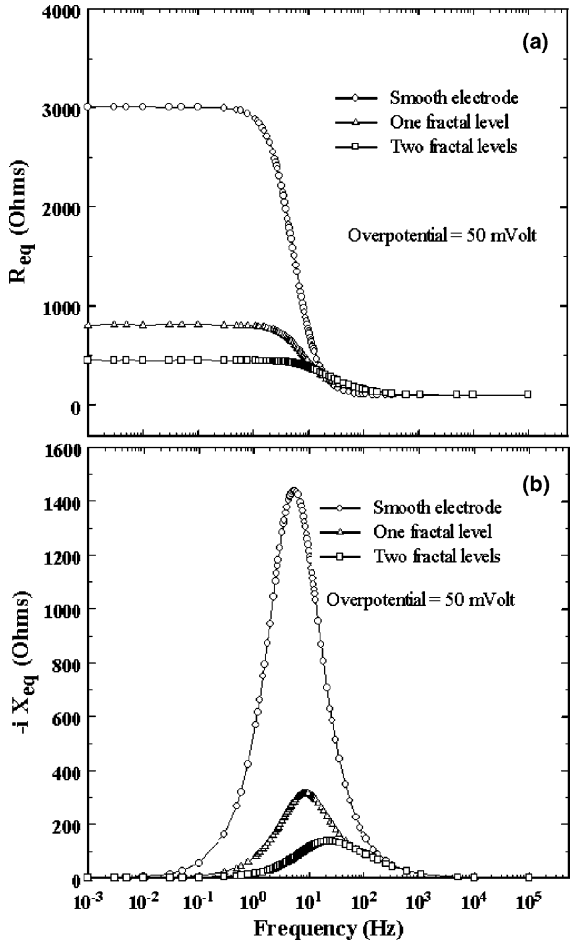

Fig. 3. R_{eq} and X_{eq} as a function of the frequency for three different fractal nets: a flat electrode and two rough electrodes. $\beta_c = 0.5$, $T = 298$ K, $R = 100\ \Omega$, $a = 4$, $C_{dl} = 1 \times 10^{-5}$ F.

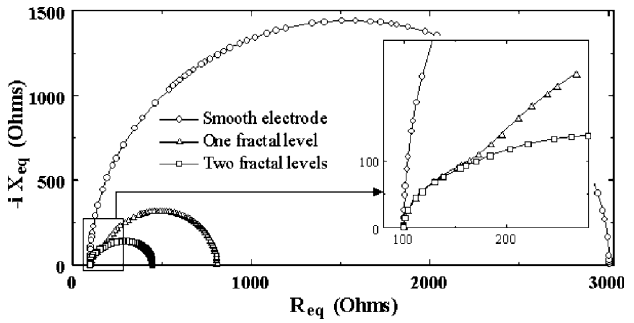

Fig. 4. Argand Diagram of the EEI for flat, one and two fractal levels electrodes. $\beta_c = 0.5$, $T = 298$ K, $R = 100\ \Omega$, $a = 4$, $C_{dl} = 1 \times 10^{-5}$ F. Overpotential = 50 mV.

the semicircles get distorted and become smaller. When rough electrodes are used, at high frequencies, the points can be adjusted to a depressed semi-circular arc equivalent to the fractal circuit without R_{ctj}. This may be appreciated in the inset of Fig. 4.

7.2. Experimental

The behavior of the resistance and the reactance as a function of the frequency of the three roughnesses is presented in Figs. 6 and 7. These diagrams are parametric in roughness. Fig. 6 shows the behavior of XR of the different electrodes. The inset shows a detail of the curve at high frequencies. It is observed that the semicircle is much smaller for the electrode with a higher roughness.

It is possible to define an apparent charge transfer resistance R_{cta}, and a double layer apparent capacity C_{dla}, similar to the ones of a flat electrode. R_{cta} is calculated from the XR diagram as the diameter of the semicircle. C_{dla} is deduced using R_{cta} and f_0 from Eq. (12).

$$C_{dla} = \frac{1}{2\pi f_0 R_{cta}} \tag{12}$$

Fig. 7a shows the behavior of R_{eq} versus frequency and Fig. 7b shows the one of X_{eq} versus frequency. The results show that we have only reached the beginning of the low frequency plateau only in the case of the electrode of higher roughness. The peak of X_{eq} curve matches the 50% of the maximum amplitude of the corresponding R_{eq} curve, for the electrode polished at 78 μm.

The data obtained were not enough to reach the plateau for the rest of the electrodes, but we can deduce from the curves, that the plateau will be placed in a lower frequency range.

8. Discussion and conclusions

A phenomenological circuit model has been used instead of *black box* model, because it allows us to interpret better the physical processes involved in the system. Therefore, each component has its specific physical interpretation.

The double layer charge can be interpreted as a molecular capacitor, where one plate is represented by the charges on the metal and the other by the ions at a minimum distance in the solution. The charge transfer process can be modulated as a variable electrical resistance, which depends on the overpotential applied to the interface.

The electrolytical channels of the fractal structure can be modulated according to several authors [13,19–25,20,26] as resistive elements.

The electrical model analysed is simple, it does not use idealized components without an specific physical interpretation as the constant phase angle element (CPA), and it reflects qualitatively the experimental results of other authors.

An important and well known aspect is that the geometry and the electrochemical processes are not independent. The current flow through the interface produces a potential drop which depends of the fractal level depth [26]. This

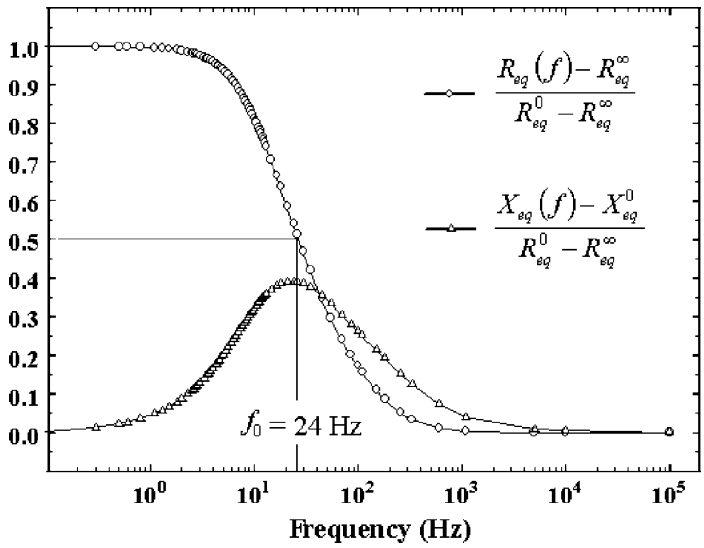

Fig. 5. Normalized R_{eq} and X_{eq} versus frequency for rough electrode modeled with two fractal levels. R_{eq}^{∞} is the value of R_{eq} for $f \to \infty$, R_{eq}^{0} is the value of R_{eq} for $f \to 0$ and f_0 is the frequency where X_{eq} presents a maximum. $\beta_c = 0.5$, $T = 298$ K, $R = 100\ \Omega$, $a = 4$, $C_{dl} = 1 \times 10^{-5}$ F and $\eta_{in}^{0} = 50$ mV.

fact is also evident in this paper since it affects the R_{ct} behavior, because it has different values depending on the fractal level analysed, as it is shown in Fig. 5 of the reference [13].

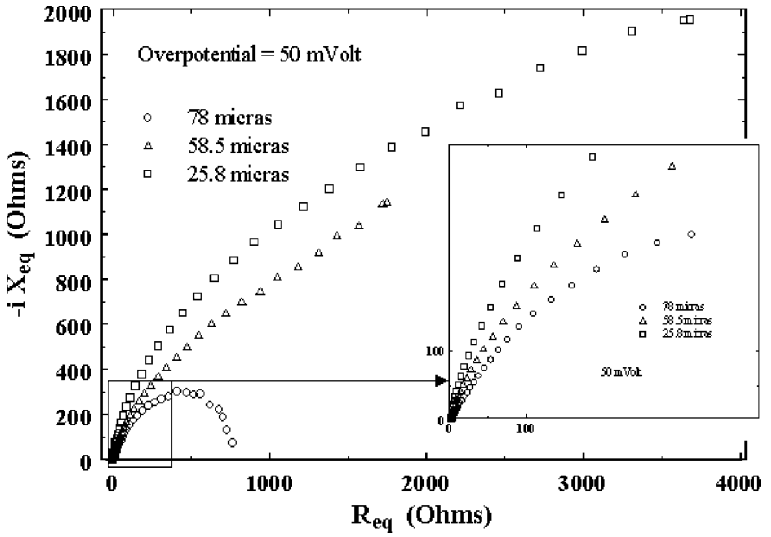

Fig. 6. Argand diagram of the EEI for AISI 304 stainless steel electrodes polished at different roughness degrees. Frequency range: 0.01 Hz–65 kHz.

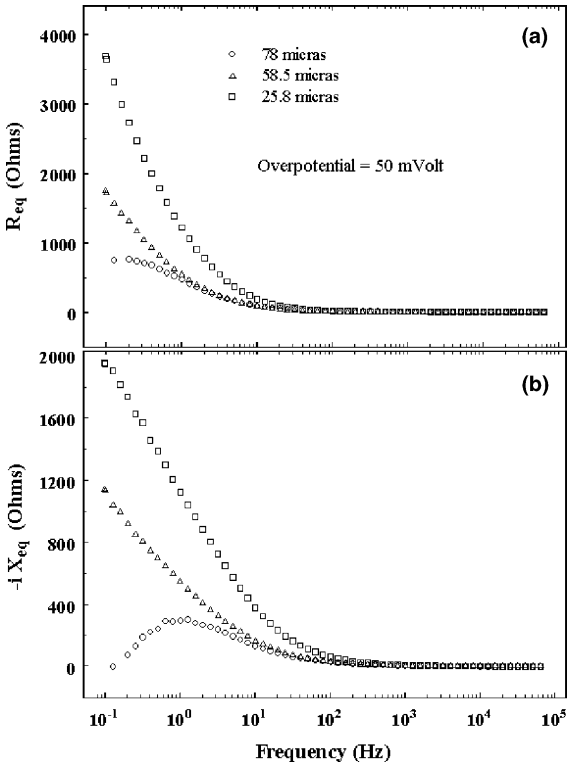

Fig. 7. Resistance (a) and reactance series equivalents (b) of the EEI versus frequency for three roughness degrees. The overpotential applied was 50 mV.

Regarding the dependence with the roughness of the impedance interface, the model predicts that, when the number of fractal levels increases (higher roughness) R_{eq} and X_{eq} decrease as it is shown in Figs. 3 and 4. It is observed qualitatively a coincidence between the behavior predicted and the experimental results (Fig. 7).

Fig. 5 shows that X_{eq} reaches the peak and R_{eq} the 50% of the maximum value when the dispersion frequency f_0 occurs. This behavior could only be obtained in our experiments for the electrode polished at 78 μm. Data at frequencies lower than 2 Hz were very hard to obtain, due to a great increase of the noise and the excessive time of the measurement which made the experimental conditions highly unstable.

The measurement noise increased particularly at low frequencies, because the integration time of each measurement had to be decreased at one cycle. When the roughness of the electrode was increased, the semicircles became smaller and R_{cta} decreased as it is shown in Fig. 4 (prediction of the model) and Fig. 6 (experimental data).

The inset of Fig. 4 shows a detail of the XR curves at high frequencies. It is possible to fit a depressed semi-circular arc in the case of rough electrodes which differs from the one made at low frequencies. This difference can be appreciated from the fact that at low frequencies, $\frac{1}{2\pi f C_{dlj}} \ll R_{ctj}$. Therefore the original circuit can be replaced by another one without R_{ctj}.

Finally, it has to be made clear that, although this model predicts qualitatively the behaviors observed, it is still incomplete. As an example, a mass transport phenomena such as diffusion [18] which is significant at low frequencies and at high overpotentials, must be incorporated.

A quantitative prediction will be attempted in further research steps. This will also involve a deeper analysis and experimentation, because the connections between some electrochemical factors such as the current density exchange and the roughness, remain still ignored.

Acknowledgements

Supported by grants from Consejo Nacional de Investigaciones Científicas y Técnicas (CONICET), the Consejo de Investigaciones de la Universidad Nacional de Tucumán (CIUNT), and Institutional funds from INSIBIO (Instituto Superior de Investigaciones Biológicas). Thanks to Santiago Caminos for his help in the translation of this paper.

References

[1] Murdock CC, Zimmerman EE. Polarization impedance at low frequency. Physics 1936;7:211–9.
[2] Schwan HP, Maczuk JG. Electrode polarization impedance: limits of linearity. In: Proceedings of the 18th ACEMB, paper 5–1, Philadelphia, PA, 1965.
[3] De Levie R. The influence of surface roughness of solid electrode on electrochemical measurements. Electrochim Acta 1965;10:113–30.
[4] Schwan HP. Alternating current electrode polarization. Biophysik 1966;3:181–201.
[5] Schwan HP. Polarization impedance and measurement in biological materials. Trans NY Acad Sci 1968;148:191–209.
[6] Geddes LA, Da Costa CP, Wise G. The impedance of stainless-steel electrodes. Med Biol Eng Comput 1971;9:511–21.
[7] Onaral B, Schwan HP. Linear and nonlinear properties of platinum electrode polarization. Part 1: Frequency dependence at very low frequency. Med Biol Eng Comput 1982;20:299–306.
[8] Hun HS, Onaral B. A unified approach to represent metal electrode polarization. IEEE Trans Biom Eng 1983;30:399–405.
[9] Bates JB, Chu YT. Electrode–electrolyte impedance: experiments and model. Ann Biomed Eng 1992;20:349–62.
[10] McAdams ET, Jossinet J. A physical interpretation of Schwan's limit current of linearity. Ann Biomed Eng 1992;20:307–19.
[11] Macdonald JR. Impedance spectroscopy. Ann Biomed Eng 1992;20:289–305.
[12] McAdams ET, Jossinet J, Lackermeier A. Modelling the constant phase angle behaviour of biological tissues: potential pitfalls. Innov Tech Biol Med 1995;16:662–70.
[13] Ruiz GA, Felice CJ, Valentinuzzi ME. Non-linear response of electrode–electrolyte interface at high current density. Chaos, Solitons & Fractals 2005;25:649–54.
[14] Davey CL, Kell DB. The influence of electrode polarisation on dielectric spectra, with special reference to capacitive biomass measurement. I. Quantifying the effects on electrode polarisation of factors likely to occur during fermentation. Bioelectrochem Bioenerg 1998;46:91–103.
[15] Woodward AM, Kell DB. On the nonlinear dielectric properties of biological systems. Bioelectrochem Bioenerg 1990;24:83–100.
[16] Blake-Coleman BC, Hutchings MJ, Silley P. Harmonic generation in 'non-linear' biological systems. Biosensors Bioelectron 1994;9(3):91–103.
[17] Ragheb T, Geddes LA. The polarization impedance of common electrode metals operated at low current density. Ann Biomed Eng 1991;19:151–63.
[18] Warburg E. Ueber das verhalten sogenanter unpolarsbarer elektroden gegen wechselstrom. Ann Phys Chim 1899;67:493–9.

[19] Liu SH. Fractal model for the ac response of a rough interface. Phys Rev Lett 1985;55:529–32.
[20] Kaplan T, Gray L. Effect of disorder on a fractal model for ac response of a rough interface. Phys Rev B 1985;32:7360–6.
[21] Kaplan T, Liu SH. Inverse-Cantor bar model for the ac response of a rough interface. Phys Rev B 1986;34:4870–3.
[22] Kaplan T, Gray L, Liu SH. Self-affine fractal model for a metal-electrolyte interface. Phys Rev B 1987;35:5379–81.
[23] Nyikos L, Pajkossy T. Fractal dimension and fractional power frequency-dependent impedance of blocking electrode. Electrochim Acta 1985;30:1533–40.
[24] Nyikos L, Pajkossy T. Diffusion to fractal surfaces. Electrochim Acta 1986;31:1347–50.
[25] Pajkossy T, Nyikos L. Impedance of planar electrodes with scale-invariant capacitance distribution. J Electroanal Chem 1992;332:55–61.
[26] De Levie R. Fractals and rough electrodes. J Electroanal Chem 1990;281:1–21.